UC San Diego

UC San Diego Previously Published Works

Title

Predominantly global genetic influences on individual white matter tract microstructure

Permalink

https://escholarship.org/uc/item/51s7j1kd

Authors

Gustavson, Daniel E

Hatton, Sean N

Elman, Jeremy A

et al.

Publication Date

2019

DOI

10.1016/j.neuroimage.2018.10.016

Peer reviewed

eScholarship.org Powered by the California Digital Library
University of California

NeuroImage 184 (2019) 871–880

Contents lists available at ScienceDirect

NeuroImage

journal homepage: www.elsevier.com/locate/neuroimage

Predominantly global genetic influences on individual white matter tract microstructure

Daniel E. Gustavson [a,b,*], Sean N. Hatton [a,b,c], Jeremy A. Elman [a,b], Matthew S. Panizzon [a,b], Carol E. Franz [a,b], Donald J. Hagler Jr. [d], Christine Fennema-Notestine [a,d], Lisa T. Eyler [a,e], Linda K. McEvoy [d], Michael C. Neale [f], Nathan Gillespie [f], Anders M. Dale [c,d], Michael J. Lyons [g], William S. Kremen [a,b,h]

[a] Department of Psychiatry, University of California, San Diego, La Jolla, CA, USA
[b] Center for Behavior Genetics of Aging, University of California, San Diego, La Jolla, CA, USA
[c] Department of Neurosciences, University of California, San Diego, La Jolla, CA, USA
[d] Department of Radiology, University of California, San Diego, La Jolla, CA, USA
[e] Mental Illness Research, Education, And Clinical Center, Veterans Affairs San Diego Healthcare System, La Jolla, CA, USA
[f] Virginia Institute for Psychiatric and Behavior Genetics, Virginia Commonwealth University, Richmond, VA, USA
[g] Department of Psychological and Brain Sciences, Boston University, Boston, MA, USA
[h] Center of Excellence for Stress and Mental Health, Veterans Affairs San Diego Healthcare System, La Jolla, CA, USA

ARTICLE INFO

Keywords:
Heritability
Diffusion tensor imaging
Genetics
Genomics
Twin study

ABSTRACT

Individual differences in white matter tract microstructure, measured with diffusion tensor imaging (DTI), demonstrate substantial heritability. However, it is unclear to what extent this heritability reflects global genetic influences or tract-specific genetic influences. The goal of the current study was to quantify the proportion of genetic and environmental variance in white matter tracts attributable to global versus tract-specific influences. We assessed fractional anisotropy (FA), mean diffusivity (MD), axial diffusivity (AD), and radial diffusivity (RD) across 11 tracts and 22 subdivisions of these tracts in 392 middle-aged male twins from the Vietnam Era Twin Study of Aging (VETSA). In principal component analyses of the 11 white matter tracts, the first component, which represents the global signal, explained 50.1% and 62.5% of the variance in FA and MD, respectively. Similarly, the first principal component of the 22 tract subdivisions explained 38.4% and 47.0% of the variance in FA and MD, respectively. Twin modeling revealed that DTI measures of all tracts and subdivisions were heritable, and that genetic influences on global FA and MD accounted for approximately half of the heritability in the tracts or tract subdivisions. Similar results were observed for the AD and RD diffusion metrics. These findings underscore the importance of controlling for DTI global signals when measuring associations between specific tracts and outcomes such as cognitive ability, neurological and psychiatric disorders, and brain aging.

1. Introduction

Diffusion tensor imaging (DTI) estimates the directionality and magnitude of the diffusion of water molecules within the brain, which aids in characterizing white matter microstructure. Findings from twin, family, and association studies have revealed that much of the variability in white matter tracts across multiple DTI metrics is influenced by genetic factors (Chiang et al., 2011; Hatton et al., 2018; Jahanshad et al., 2013; Kochunov et al., 2016; Lee et al., 2017; Vuoksimaa et al., 2017). However, it is unclear to what extent these genetic influences are due to (i) unique factors specific to each tract, or (ii) general variance in white matter across the entire brain. Greater understanding of the genetic and environmental influences on white matter structure may expedite ongoing efforts to use genome-wide association studies to identify the genetic influences on white matter microstructure (Hatton et al., 2018). This knowledge in turn could improve our understanding of associations between white matter microstructure and outcomes such as cognitive ability, psychiatric disorders, and brain aging.

Fractional anisotropy (FA) quantifies directional diffusion within a voxel and is broadly used to describe the density and coherence of a

* Corresponding author. Department of Psychiatry, University of California San Diego, 9500 Gilman Dr. (MC 0738), La Jolla, CA, 92093, USA.
E-mail address: dgustavson@ucsd.edu (D.E. Gustavson).

https://doi.org/10.1016/j.neuroimage.2018.10.016
Received 16 May 2018; Received in revised form 6 August 2018; Accepted 4 October 2018
Available online 5 October 2018
1053-8119/© 2018 Elsevier Inc. All rights reserved.

white matter region. Higher FA indicates stronger directionality and better cohesion of white matter. In contrast, mean diffusivity (MD) represents the average diffusivity of water molecules within a voxel, regardless of direction, and is used in the clinical diagnosis and characterization of lesions (Alexander et al., 2007). As white matter develops, FA increases and MD decreases in healthy populations until early adulthood, followed by steady decreases in FA and increases in MD throughout the rest of the lifespan (Westlye et al., 2010). Lower white matter FA and higher white matter MD have also been associated with lower cognitive functioning (Bennett and Madden, 2014; Charlton et al., 2006; Mabbott et al., 2006).

Axial diffusivity (AD) and radial diffusivity (RD), respectively, reflect the magnitude of diffusion of water along, or perpendicular to, the primary axis of directionality, and are used in the computation of FA and MD (for review, see Alexander et al., 2011). Murine models suggest that reduced myelin due to dysmyelination or demyelination is associated with increased RD and reduced AD (Harsan et al., 2006; Song et al., 2002, 2005; Tyszka et al., 2006). Further murine models of reversible dysmyelination (Harsan et al., 2006; Sun et al., 2006) show that decreases in AD are associated with reduced axonal caliber and increased expression of the cytoskeletal proteins, whereas increases in AD are associated with increases in axonal number and caliber. Thus, it is generally accepted that decreases in AD reflect disorganization, damage, or loss of axons (Freund et al., 2012; Song et al., 2005; Tyszka et al., 2006; Zhang et al., 2009), and that increases in RD are a result of disruptions to the myelin sheath (Chen et al., 2011; Klawiter et al., 2012; Naismith et al., 2010; Song et al., 2002). All of these factors influence MD.

Twin studies have shed light on the genetic/environmental architecture of white matter and suggest that much of the variance between people in DTI-derived measures in any given white matter tract can be explained by genetic influences. For example, in previous research using the same sample described here (men ages 56–66 years) heritability estimates were high for all four diffusivity indices in 12 bilateral white matter tracts and the corpus callosum (Vuoksimaa et al., 2017). Although heritability estimates of global measures were especially high (0.72-0.80), the estimates varied considerably between tracts. For example, of the tracts assessed in the present study, heritabilities of FA measures were 0.50–0.82 for 87% of the tracts and 0.28-0.46 for the remaining 13%. These results were consistent with estimates based on voxel-wise analyses of FA, which also suggested that heritability may be higher in adolescents than young adults, and higher in males than females (Chiang et al., 2011). However, because Chiang et al.'s adolescent heritability estimate was based on a small sample, replication using a much larger sample is required to confirm this age-related trend. More recent findings suggest that the genetic influences on AD and RD within a given tract are moderately correlated (Hatton et al., 2018).

Thus, genetic influences account for most of the variance in white matter microstructure across the brain and within localized anatomical regions, but a remaining question concerns the underlying structure of the phenotypic and genetic/environmental influences on individual differences in white matter morphometry. For example, a set of common genetic and/or environmental influences may contribute to white matter microstructure across the entire brain, such as factors that influence myelination and cellular structure (Alexander et al., 2011). If a general factor (e.g., the first principal component of a PCA) explains considerable variance across all white matter tracts, it will be important to identify the extent to which genetic and environmental influences on a given tract are explained by this general factor. It will also be important to quantify the amount of genetic and environmental influences that are unique to a tract, as this localized variance will be important when examining how specific tracts are associated with outcomes such as cognitive ability, psychiatric disorders, motor function, and brain aging (beyond those associations with white matter microstructure across the entire brain).

We used two approaches to examine global and specific influences on heritability of white matter tracts. First, to examine evidence for a global factor, we conducted principal components analysis of white matter microstructural measures within 11 white matter tracts and 22 tract subdivisions representing anatomically meaningful sub-regions of 8 of the white matter tracts. We hypothesized that the first principal component would explain much (if not most) of the variance across all tracts or tract subdivisions.

Second, we examined the genetic/environmental correlations between global measures of FA or MD and the same measures within 11 individual white matter tracts or 22 subdivisions using bivariate twin analyses. These twin analyses statistically parse the total variance in each dependent measure (and its covariance with global measures) into three sources of influences: genetic influences (i.e., the sum of all effects of additive genetic influences across the genome), shared environmental influences (influences that make twins in a pair similar to one another), and nonshared environmental influences (influences that make twins in a pair different from one another, including measurement error). Thus, these analyses quantify the extent to which genetic/environmental influences are specific to a given tract or subdivision, or reflect influences that are common to global diffusion measures that represent the brain's white matter microstructure as a whole. We hypothesized that a large proportion of the genetic variance in white matter tracts would be explained by genetic influences on the global measure, but there will also be genetic influences specific to individual tracts. Finally, we conducted parallel genetic analyses for the AD and RD diffusion metrics, from which FA and MD are calculated. AD and RD share some genetic variance but there are also some genetic influences that are unique to each (Hatton et al., 2018). These analyses are mostly described in the supplementary material.

2. Methods

2.1. Subjects

Data analyses were based on 390 male twins who participated in the second wave of the longitudinal Vietnam Era Twin Study of Aging (VETSA) project and had adequate DTI data. The sample included 84 full monozygotic (MZ) twin pairs, 56 full dizygotic (DZ) twin pairs, and 110 unpaired twins. VETSA participants were recruited randomly from a previous study of members of the Vietnam Era Twin Registry (Tsuang et al., 2001). All individuals served in the United States military at some time between 1965 and 1975, but nearly 75% reported no combat

Table 1
Sample characteristics.

Characteristic	N	M	SD	Range
Age	390	61.82	2.62	56, 66
Lifetime education	389	13.76	2.10	5, 20
Occupation	388	5.45	1.78	0, 9
Ethnicity (% white nonHispanic)	390	86.67	*na*	*na*
Combat Exposure (% yes)	334	26.34	*na*	*na*
Traumatic Brain Injury (% yes)	381	27.30	*na*	*na*
PTSD symptoms	389	25.17	9.63	17, 74
Alcohol Use Problems	358	0.98	1.15	0, 4

Note: Lifetime education was the number of years of school completed. Occupation was based on the Hollingshead Four-Factor index (Hollingshead, 1975), from 0 (unemployed) to 9 (major professionals). Combat exposure was assessed as part of an earlier study (at approximately age 41) with the Combat Exposure Index (Janes et al., 1991; Koenen et al., 2003). Traumatic brain injury was based on an interview centered around responses to three questions regarding whether they were ever told they had a concussion by a doctor, or had a severe head injury that was associated with loss of consciousness or confusion (Kaup et al., 2018). Post-traumatic stress disorder (PTSD) symptoms were based on the 17-item DSM-IV based PTSD checklist civilian version (Weathers et al., 1993). 3.3% of the sample reported scores greater than 49, a good predictor of PTSD diagnosis (Weathers et al., 1993). Alcohol problems were assessed with The CAGE Questionnaire (Mayfield et al., 1974), with 3.1% of respondents received scoring 4 (an indicator of alcoholism) and 27.1% of respondents reporting scores of 2 or 3 (indicating potential alcohol problems).

exposure. Sample characteristics are displayed in Table 1. Participants are generally representative of American men in their age group with respect to health and lifestyle characteristics (Kremen et al., 2006, 2011; Schoenborn and Heyman, 2009).

Data were collected at the University of California, San Diego (UCSD) and Boston University (BU). MRI data collection for BU participants was conducted at the Massachusetts General Hospital (MGH). All participants gave their written informed consent before participation, and the study protocol was approved by the Institutional Review Boards at all participating institutions.

2.2. Image acquisition

Image acquisition, processing, and generation of the DTI measures in this sample have been previously described (Hatton et al., 2018; McEvoy et al., 2015; Vuoksimaa et al., 2017), and are briefly summarized here. T1-weighted and diffusion-weighted images were acquired on 3T scanners at both sites; twin pairs were always assessed on the same scanner. At UCSD, images were acquired on a GE 3T Discovery 750 scanner (GE Heath-care, Waukesha, WI, USA) with an eight-channel phased array head coil. The imaging protocol included a sagittal 3D fast spoiled gradient echo (FSPGR) T1-weighted image (TE = 3.164 ms, TR = 8.084 ms, TI = 600 ms, flip angle = 8°, pixel bandwidth = 244.141, FOV = 24 cm, frequency = 256, phase = 192, slices = 172, slice thickness = 1.2 mm), and a diffusion-weighted image with 51 diffusion directions, b value = 1000 s/mm^2, integrated with a pair of b = 0 images with opposite phase-encode polarity, TR = 9700 ms, TE = 80–84 ms, pixel bandwidth = 3906.25. Acquisition resolution for diffusion scans was 2.5 mm isotropic, but images written by the scanner had a nominal resolution of 1.875 × 1.875 × 2.5 mm.

At MGH, images were acquired with a Siemens Tim Trio (Siemens USA, Washington, DC) with a 32-channel head coil. The imaging protocol included a 3D magnetization-prepared rapid gradient echo (MPRAGE) T1-weighted image (TE = 4.33 ms, TR = 2170 ms, T1 = 1100 ms, flip angle = 7°, pixel bandwidth = 140, slices = 160, slice thickness = 1.2 mm), and a diffusion-weighted image consisting of two separate b = 0 images with opposite phase-encode polarity, followed by two scans with 30 diffusion directions, b value = 1000 s/mm^2 (and one b = 0 image), TR = 9500 ms, TE = 94 ms, pixel bandwidth = 1371. Acquisition resolution for diffusion scans was 2.5 mm isotropic, and images written by the scanner had the same resolution.

2.3. Image processing

Images were processed at the Center for Multimodal Imaging Genetics (CMIG) as described previously (McEvoy et al., 2015; Vuoksimaa et al., 2017). Briefly, T1-weighted (T1) structural images were corrected for gradient nonlinearity distortions (Jovicich et al., 2006) and B1 field inhomogeneity (Sled et al., 1998) and then rigidly resampled and registered to standard space. Diffusion MRI (dMRI) data were corrected for eddy current distortion (Zhuang et al., 2006), head motion (Hagler et al., 2009), B0 distortions (Holland et al., 2010), and gradient nonlinearity distortions (Jovicich et al., 2006). The b = 0 images were registered to T1 images using mutual information (Wells et al., 1996). That registration was used to rigidly resample the dMRI data into a standard orientation relative to the atlas-registered T1, with 2 mm isotropic resolution. All images were visually inspected to exclude data with severe scanner artifacts or excessive head motion. We excluded an additional 42 individuals from the analyses based on this data quality review, as reported in our earlier work (Vuoksimaa et al., 2017).

2.4. DTI measures

We previously reported the process of identifying 25 white matter fiber tracts, 12 in each hemisphere plus the corpus callosum (Vuoksimaa et al., 2017) using a probabilistic atlas which estimated the *a posteriori* probability that a voxel belongs to a particular fiber tract (AtlasTrack; Hagler et al., 2009). Fiber probability maps were used to create a weighted average across all voxels within a region of interest (i.e., each tract). We collapsed tracts by averaging DTI measures across the left and right hemispheres because we have demonstrated that heritabilities were similar across left and right hemispheres for all tracts (Vuoksimaa et al., 2017), resulting in 12 tracts plus the corpus callosum. We excluded the corticospinal tracts from the present investigation due to low reliability (i.e., because the volume and average diffusivity measures can vary solely due to the variations in the size of the participant's head with respect to the fixed field of view of the acquisition matrix). The fornix was also excluded because segments of this fine structure are smaller than the voxel size used and lie along the third ventricle, often leading to error-prone estimations due to co-registration and partial voluming. Thus, 11 tracts were used here (anterior thalamic radiation, corpus callosum, cingulate gyrus portion of the cingulum, hippocampal portion of the cingulum, inferior frontal occipital fasciculus, inferior frontal superior frontal cortex, inferior longitudinal fasciculus, superior corticostriate, superior longitudinal fasciculus, striatal inferior frontal cortex, and uncinate). Dependent measures were residualized to account for the use of different scanners across sites (UCSD or BU). These 11 tracts are shown in Fig. 1 (excluding the corpus callosum due to its large size).

Eight of these fiber tracts (those tracts included in AtlasTrack; Hagler et al., 2009): anterior thalamic radiation, corpus callosum, cingulum (cingulate gyrus portion), cingulum (hippocampal portion), inferior frontal occipital fasciculus, inferior longitudinal fasciculus, superior longitudinal fasciculus, and uncinate) were segmented into subdivisions. The method of fiber tract segmentation has been described in detail previously (Hagler et al., 2009). Briefly, spatial subdivisions of each of these tracts were manually defined as a series of binary mask volumes in the space of the probabilistic atlas. For example, the inferior frontal occipital fasciculus was divided along the posterior-anterior axis into three parts, whereas the uncinate fasciculus was divided into temporal and frontal parts. These masks were morphed from atlas-space into individual subject-space, using the nonlinear registration used to align a subject to the atlas. The fiber tract probability maps for each of the complete tracts were then multiplied by the sub masks, creating subdivision probability maps for each subject, which were then used to calculate weighted averages of the DTI measures, as was done for the full fiber tracts.

Although the distributions of each subdivision were marginally skewed, we identified some extreme outliers (1 total observation for FA, 26 total observations across 12 subdivisions for MD) with values more than three times the interquartile range above the upper quartile. These cases were reviewed again to verify no technical errors related to image processing, and the values were trimmed to three times the interquartile range above the upper quartile (see Table 2 for descriptive statistics). Analyses were also conducted on the raw data and revealed qualitatively similar results.

2.5. Data analysis

Principal components analysis. Principal components analyses were conducted in SPSS (version 24) with no rotation. Missing data were excluded in a pair-wise manner. We used scree plots to inform the analysis, but all factors with an eigenvalue >1 were extracted.

Genetic analyses. We conducted biometrical genetic twin analyses using the structural equation modeling package OpenMx (version 2.7.9) in R version 3.3.3 (Neale et al., 2016). OpenMx accounts for missing observations using a full-information maximum likelihood approach.

Genetic models were based on the standard assumptions of the classical twin design (Neale and Cardon, 1992), in which the variance of a phenotype can be separated into proportions attributable to additive genetic influences (A), common environmental influences (C), and non-shared environmental influences (E). Genetic influences (A) are assumed to correlate at 1.0 in MZ twin pairs because they share 100% of their alleles identical-by-descent. The DZ twin pair correlation is assumed

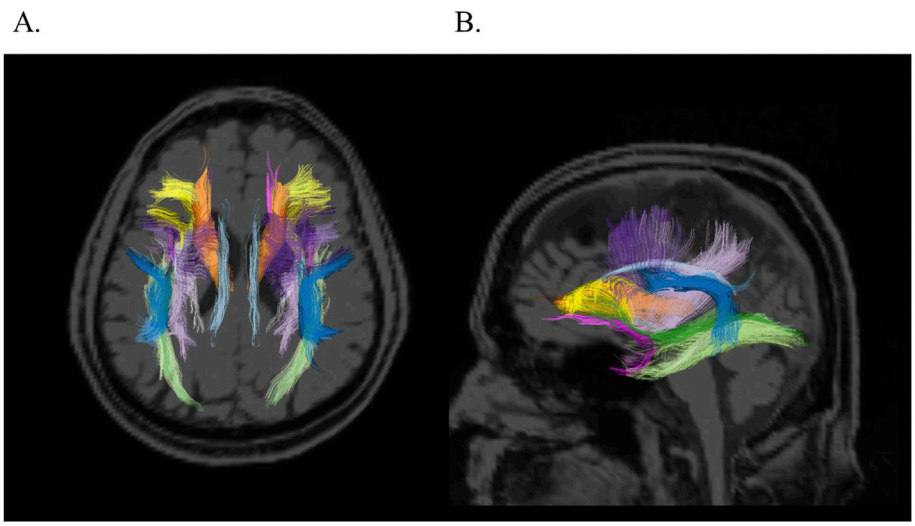

Fig. 1. The 11 white matter tracts analyzed in the current study, shown for an example subject. The corpus callosum was excluded from this example because its size makes it difficult to see other tracts. Axial (A) and sagittal (B) views are displayed. Anterior thalamic radiation (orange), Cingulum, cingulate gyrus portion (light blue), Cingulum, hippocampal portion (white), Inferior frontal occipital fasciculus (dark green), Inferior frontal superior frontal cortex (dark purple), Inferior longitudinal fasciculus (light green), superior corticostriate (light purple), Superior longitudinal fasciculus (dark blue), Striatal inferior frontal cortex (yellow), Uncinate (pink).

to be 0.5 in because DZs, on average, share 50% of their alleles identical-by-descent. Shared environmental influences (C), which are influences that make twins more similar, are assumed to be correlated at 1.0 in both MZ and DZ twins. Non-shared environmental influences (E) are specified to correlate 0 in both MZ and DZ twins, and necessarily includes measurement error. This method also assumes equal means and variances within twin pairs and across zygosity. These assumptions for univariate analyses also apply in bivariate analyses. As in other structural equation models, latent genetic/environmental variance components were not measured directly. Rather, these assumptions were imposed on the model and the maximum likelihood estimator converged on the best-fitting solution.

Table 2
Descriptive statistics for fractional anisotropy and mean diffusivity in all 11 tracts and 22 tract subdivisions.

Tracts	Fractional Anisotropy (FA)				Mean Diffusivity (MD)			
	M	*SD*	Range	Skewness	*M*	*SD*	Range	Skewness
All Fibers	0.46	0.02	.40, .50	−0.33	0.84	0.03	.77, .96	0.71
Tracts								
Anterior thalamic radiation	0.40	0.03	.31, .48	−0.23	0.82	0.04	.74, 1.00	1.23
Corpus callosum	0.52	0.03	.43, .58	−0.25	0.89	0.04	.80, 1.05	0.69
Cingulum, cingulate gyrus portion	0.49	0.04	.37, .60	−0.18	0.75	0.03	.69, .83	0.46
Cingulum, hippocampal portion	0.35	0.03	.25, .46	−0.04	0.83	0.05	.73, 1.07	1.29
Inferior frontal occipital fasciculus	0.46	0.02	.38, .53	−0.08	0.86	0.04	.77, 1.00	0.53
Inferior frontal superior frontal cortex	0.40	0.02	.32, .46	−0.44	0.75	0.03	.68, .92	1.11
Inferior longitudinal fasciculus	0.45	0.02	.37, .53	−0.07	0.84	0.04	.75, .98	0.48
Superior corticostriate	0.46	0.03	.38, .53	−0.22	0.75	0.03	.69, .89	1.18
Striatal inferior frontal cortex	0.40	0.02	.33, .45	−0.11	0.78	0.03	.70, 98	1.02
Superior longitudinal fasciculus	0.45	0.03	.34, .52	−0.45	0.75	0.03	.69, .93	1.33
Uncinate	0.41	0.03	.29, .49	−0.40	0.82	0.03	.75, 1.04	1.00
Tract Subdivisions								
ATR anterior	0.37	0.03	.25, .47	−0.06	0.84	0.06	.72, 1.09	1.34
ATR posterior	0.42	0.03	.33, .48	−0.25	0.80	0.04	.71, .99	1.25
CC anterior	0.47	0.03	.36, .56	−0.16	0.91	0.06	.75, 1.12	0.53
CC middle-anterior	0.51	0.03	.38, .58	−0.44	0.89	0.05	.78, 1.11	0.78
CC middle-posterior	0.52	0.03	.40, .60	−0.44	0.89	0.05	.78, 1.09	0.81
CC posterior	0.57	0.04	.44, .66	−0.64	0.90	0.09	.77, 1.24	1.49
CgC anterior	0.42	0.05	.23, .54	−0.19	0.78	0.04	.63, .87	−0.32
CgC middle	0.52	0.04	.37, .64	−0.28	0.75	0.03	.67, .84	0.34
CgC posterior	0.46	0.04	.33, .57	−0.26	0.75	0.03	.67, 84	0.70
CgH anterior	0.36	0.04	.26, .47	−0.16	0.83	0.06	.71, 1.08	1.37
CgH posterior	0.33	0.04	.16, .47	−0.37	0.82	0.06	.74, 1.04	1.44
ILF anterior	0.37	0.03	.29, .45	0.10	0.81	0.04	.72, .93	0.32
ILF middle	0.49	0.03	.38, .56	−0.08	0.84	0.04	.76, 1.03	0.73
ILF posterior	0.47	0.03	.37, .58	−0.02	0.85	0.06	.74, 1.06	0.88
IFO anterior	0.41	0.03	.31, .50	−0.13	0.79	0.03	.71, .92	0.71
IFO middle	0.49	0.03	.41, .56	−0.10	0.86	0.04	.79, 1.00	0.56
IFO posterior	0.48	0.04	.38, .58	−0.06	0.92	0.07	.77, 1.19	0.86
SLF temporal stem	0.48	0.04	.37, .57	−0.20	0.76	0.04	.68, .93	0.72
SLF parietal stem	0.45	0.03	.32, .53	−0.49	0.76	0.04	.68, .91	1.08
SLF frontal stem	0.45	0.03	.34, .53	−0.30	0.75	0.03	.68, .88	0.91
Unc frontal	0.43	0.03	.29, .54	−0.40	0.80	0.03	.73, .93	0.66
Unc temporal	0.40	0.03	.29, .48	−0.08	0.84	0.04	.75, 1.02	0.63

Note: ATR = Anterior thalamic radiation, CC = Corpus callosum, CgC = Cingulum, cingulate gyrus portion, CgH = Cingulum, hippocampal portion, IFO = Inferior frontal occipital fasciculus, IFSFC = Inferior frontal superior frontal cortex, ILF = Inferior longitudinal fasciculus, SCS = Superior corticostriate, SLF = Superior longitudinal fasciculus, SIFC = Striatal inferior frontal cortex, Unc = Uncinate.

Figure 2 provides an example of a bivariate Cholesky decomposition used to separate global and specific genetic and environmental influences in the current study. Variance in global FA is decomposed into its genetic (A_{Glob}), shared environmental (C_{Glob}), and non-shared environmental (E_{Glob}) components. Variance in the measure of FA from each candidate tract is decomposed into genetic/environmental variance shared with global white matter microstructure (A_{Glob}, C_{Glob}, E_{Glob}; paths a12, c12, e12), and genetic/environmental variance specific to that tract (A_{Spec}, C_{Spec}, E_{Spec}; paths a22, c22, e22). The total variance explained by each latent genetic/environmental factor is computed by squaring the path coefficient or loading on the latent factor, whereas genetic correlations (r_g) are computed by dividing the genetic covariance between tract FA and global FA (path a11*a12) by the square root of the product of their genetic variances ($\sqrt{(a11*11*(a12*a12 + a22*a22))}$). Thus, a standard phenotypic correlation represents the shared total variance between two phenotypes whereas the genetic correlation represents only the shared genetic variance between two phenotypes. We do not report model fit statistics for each Cholesky decomposition, but note that all models had acceptable fit (based on the difference in the −2 x log likelihood values between the best fitting a saturated model). Significance of individual parameters was established with chi-square difference tests (χ^2). 95% confidence intervals (95% CIs) were also computed for the squared paths representing proportions of genetic and environmental influences shared with global white matter microstructure (paths a12, c12, e12), and specific to that tract (paths a22, c22, e22).

3. Results

Descriptive statistics for FA and MD in all tracts and tract subdivisions are displayed in Table 2.

3.1. Evidence for a substantial global factor for FA and MD

As expected, the first principal component revealed evidence of a global factor. For the 11 tract-based measures, the first principal component explained 50.3% and 62.5% of the total variance in FA and MD, respectively. The factor loadings on each first principal component were substantial for all white matter tract subdivisions (range = 0.39 to 0.88, median = 0.74 for FA; range = 0.40 to 0.91, median = 0.84 for MD).

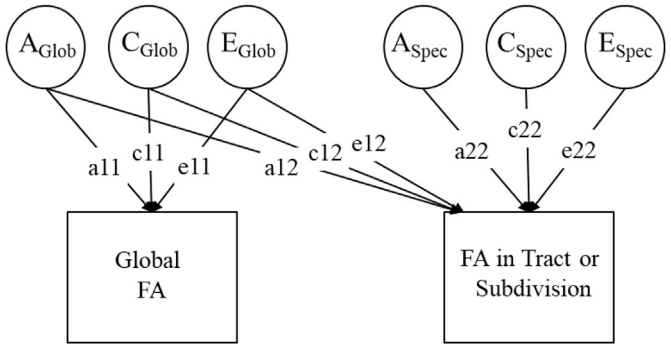

Fig. 2. Cholesky factor model used to examine the genetic/environmental influences on white matter microstructure for a given tract explained by the global measure. Genetic influences (A_{Glob}), shared environmental influences (C_{Glob}), and non-shared environmental influences (E_{Glob}) account for all the variation in the global measure of FA (estimated paths a11, c11, and e11). These influences also account for some of the FA variance in a specific tract or tract subdivision (estimated paths a12, c12, and e12), and the remaining variance in the tract FA is captured by tract-specific genetic/environmental influences (A_{Spec}, C_{Spec}, E_{Spec}; estimated paths a22, c22, and e22). The proportion of variance explained by each latent genetic/environmental factor (displayed in Figs. 3 and 4) is computed by squaring the factor loading on that factor. And the genetic correlation is computed by dividing the genetic covariance between tract FA and global FA (path a11*a12) by the total genetic variance ($\sqrt{(a11*11*(a12*a12 + a22*a22))}$).

Principal component analyses were also conducted on the 22 tract subdivisions. The first component accounted for 38.4% and 47.0% of the variance in FA and MD, respectively. Again, the factor loadings on each first component were substantial for all white matter tract subdivisions (range = 0.28 to 0.75, median = 0.65 for FA; range = 0.40 to 0.87, median = 0.69 for MD). Principal component loadings are shown in the supplement (Tables S1-S4).

Second, as shown in the supplement (Tables S5-S6), there were strong phenotypic correlations between each of the 11 FA and MD tracts and the global measures of FA and MD (r = 0.34 to 0.88, median = 0.71 for FA; r = 0.42 to 0.86, median = 0.82 for MD). Similarly, there were strong correlations between global measures and each of the 22 tract subdivisions (r = 0.29 to 0.79, median = 0.59 for FA; r = 0.30 to 0.83, median = 0.66 for MD; Tables S9 and S10). These results support our use of the global measure of FA and MD in further analyses and suggest that much, but not all, of the variance in any given white matter tract subdivision can be accounted for by variance common to all tracts.

3.2. Global measures account for about half of the tract-based genetic and environmental variance

Heritability of DTI measures based on the 11 individual white matter tracts and the proportions of variance shared with the global measures are displayed in Fig. 3. Similar results for the tract subdivisions are displayed in Fig. 4. Heritability point estimates representing variance shared with global measures (a_{global}) and variance unique to each tract ($a_{specific}$), and the corresponding 95% confidence intervals, are reported in Table 3 (FA and MD) and Table 4 (AD and RD) for white matter tracts and in the supplemental materials for tract subdivisions (Tables S13 and S14). Total heritability point estimates (i.e., global + specific genetic influences) along with genetic and environmental correlations between the global measures and each of the individual tracts and tract subdivisions are detailed in the supplemental materials, including results for AD and RD (Figures S1 and S2, and Tables S5-S12).

FA. As shown in Fig. 3a, over half of the genetic influences on a given tract ($a^2_{global} + a^2_{specific}$) could be attributed to the global FA (a^2_{global}; light blue). Genetic influences on global FA accounted for an average of 37.4% of the variance in any given tract (range in a^2_{global} = 0.06 to 0.64), and were significant for all tracts. Another 32.7% of the variance, on average, was explained by genetic influences specific to each measure (range in $a^2_{specific}$ = .17 to .50; dark blue). For example, the corpus callosum (CC) and the inferior frontal superior frontal cortex (IFSFC) were the most strongly explained by the global FA (a^2_{global} = 0.64 and 0.54, respectively), whereas the cingulate portion of the cingulum (CgC) and hippocampal portion of the cingulum (CgH) had the strongest evidence for specific genetic influences (both $a^2_{specific}$ = .50). On average, non-shared environmental influences on total variance in tracts' FA were 8.9% due to the global factor (range e^2_{global} = 0.05 to 0.15; light orange), and 14.5% specific to each tract (range $e^2_{specific}$ = .05 to .37; dark orange). Shared environmental influences accounted for a small and nonsignificant portion the total variance in each tract (average c^2_{global} = 0.07, $c^2_{specific}$ = .00).

As displayed in Fig. 4a, results were comparable for FA in tract subdivisions. Close to half the total genetic variance ($a^2_{global} + a^2_{specific}$) for FA on a given tract subdivision was explained by genetic influences on the global FA measure (average a^2_{global} = 0.30, $a^2_{specific}$ = .37). Non-shared environmental influences were largely specific to subdivisions of tracts (average e^2_{global} = 0.07, $e^2_{specific}$ = .22), and shared environmental influences were minimal and nonsignificant (average c^2_{global} = 0.04, $c^2_{specific}$ = .01).

MD. Similar results were observed for MD, although the estimated effects of the global factor appeared to account for a larger portion of the total variance than was the case for FA. As displayed in Fig. 3b, global MD accounted for an average of 50.2% of the total variance in any given tract (range in a^2_{global} = 0.17 to 0.63), with additional genetic influences accounting for on average 23.7% of the variance (range in $a^2_{specific}$ = .17 to

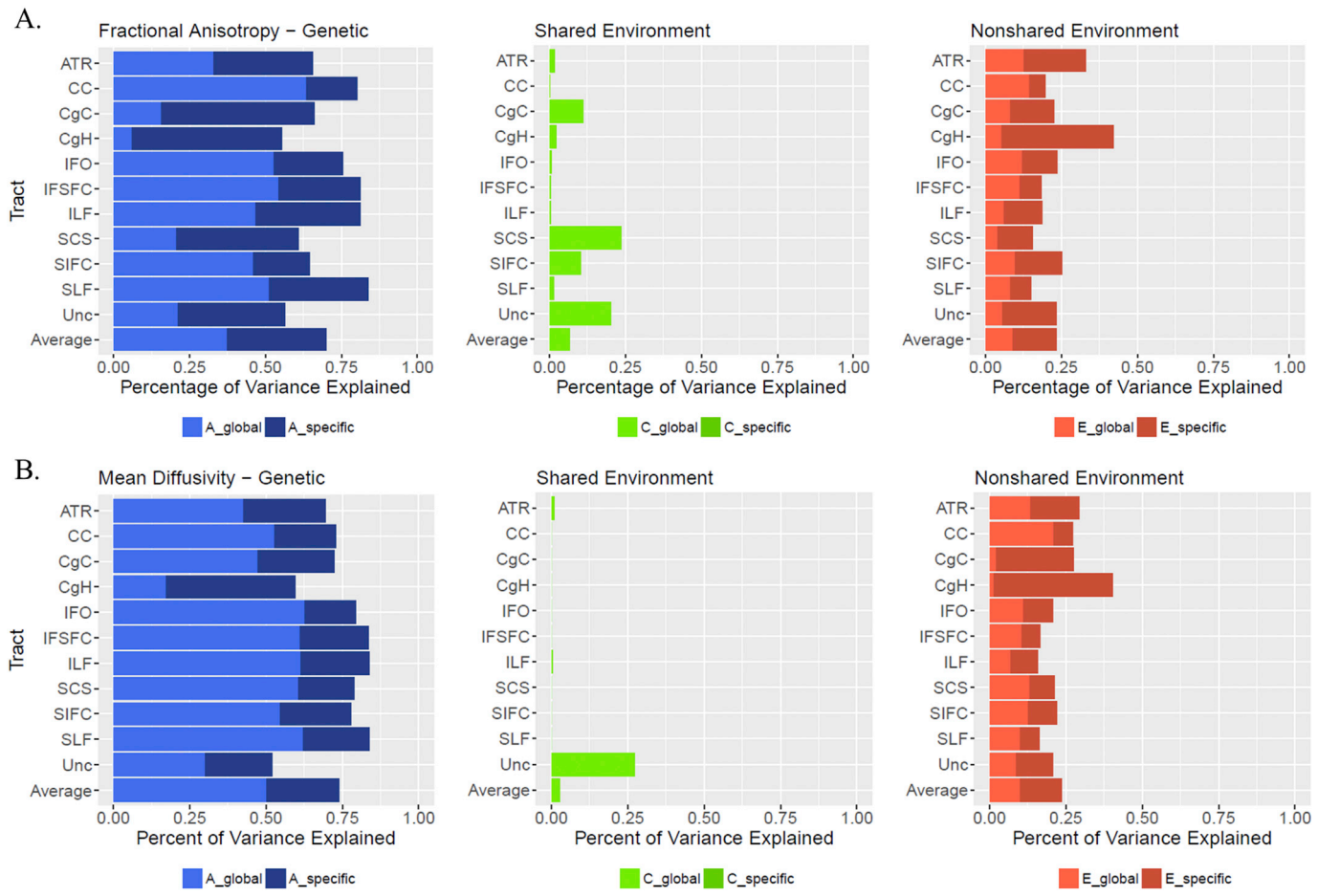

Fig. 3. Summary of the genetic (A), shared environmental (C), and non-shared environmental influences (E) on each of the 11 white matter tracts. For each type of influence, the percent of the variance explained is broken down further into the genetic/environmental influences shared with the global measure (lighter color), and the genetic/environmental influences unique to the tract (darker color). A. Results for fractional anisotropy (FA). B. Results for mean diffusivity (MD). In each histogram, the bottom row displays the mean results for all tracts. The heritability estimates, and the genetic and environmental correlations between global FA/MD and tract FA/MD are displayed in the supplement (Tables S5 and S6). Similar results are displayed for axial and radial diffusivity in the supplement (Figure S1 and Tables S7 and S8). ATR = Anterior thalamic radiation, CC = corpus callosum, CgC = Cingulum, cingulate gyrus portion, CgH = Cingulum, hippocampal portion, IFO = Inferior frontal occipital fasciculus, IFSFC = Inferior frontal superior frontal cortex, ILF = Inferior longitudinal fasciculus, SCS = superior corticostriate, SLF = Superior longitudinal fasciculus, SIFC = Striatal inferior frontal cortex, Unc = Uncinate.

.42). Thus, about two-thirds of the total genetic variance on a given tract was explained by global MD. Non-shared environmental influences were explained by both global and specific influences (average $e^2_{global} = 0.10$, $e^2_{specific} = .13$). Again, shared environmental influences were nonsignificant (average $c^2_{global} = 0.03$, $c^2_{specific} = .00$).

Analyses of tract subdivisions in Fig. 4b revealed similar patterns of results. Over half the genetic influences were explained by global MD (average $a^2_{global} = 0.35$, $a^2_{specific} = .29$). Again, there were small but significant non-shared environmental influences (average $e^2_{global} = 0.09$, $c^2_{specific} = .22$), whereas shared environmental influences were nonsignificant (average $c^2_{global} = 0.05$, $c^2_{specific} = .00$).

AD and RD. Results for AD and RD were similar to those for FA and MD (see Table 4, Figures S1-S4). Global AD accounted for an average of 39.0% of the total variance in any given tract (range in $a^2_{global} = 0.17$ to 0.54), with additional genetic influences accounting for on average 32.6% of the variance (range in $a^2_{specific} = .24$ to .57). Global RD accounted for an average of 45.5% of the total variance in any given tract (range in $a^2_{global} = 0.07$ to 0.59), with additional genetic influences accounting for an additional 25.7% of the variance, on average (range in $a^2_{specific} = .17$ to .35). Thus, the results for AD were more similar to those for FA (about half of the genetic influences explained by global measures) and the results for RD were more similar to those for MD (about two-thirds of the genetic influences were explained by global measures). Analyses for tract subdivisions followed a similar pattern, with genetic variance in global measures explaining a slightly less proportion of the variance in a given tract subdivision.

4. Discussion

The goal of the study was to better understand the genetic and environmental etiology of white matter microstructure, especially the contribution of global versus tract-specific genetic/environmental influences on FA or MD. The first principal component explained over half of the variance in FA or MD across 11 tracts, and almost half of the variance in the 22 tract subdivisions. Genetic influences accounted for the largest portion of the total variance in any given tract or tract subdivision, with over half the genetic influences on a given tract being explained by the global measures. These patterns of results were consistent across FA, MD, AD, and RD, with the results for AD slightly more similar to those for FA and the results for RD more similar to those for MD.

Global white matter measures are presumed to reflect factors that influence all white matter such as myelination and cellular structure (Alexander et al., 2011). By extension, it is reasonable to expect that individual white matter structures have a common, but not necessarily identical, set of genetic influences. Genetic influences unique to each

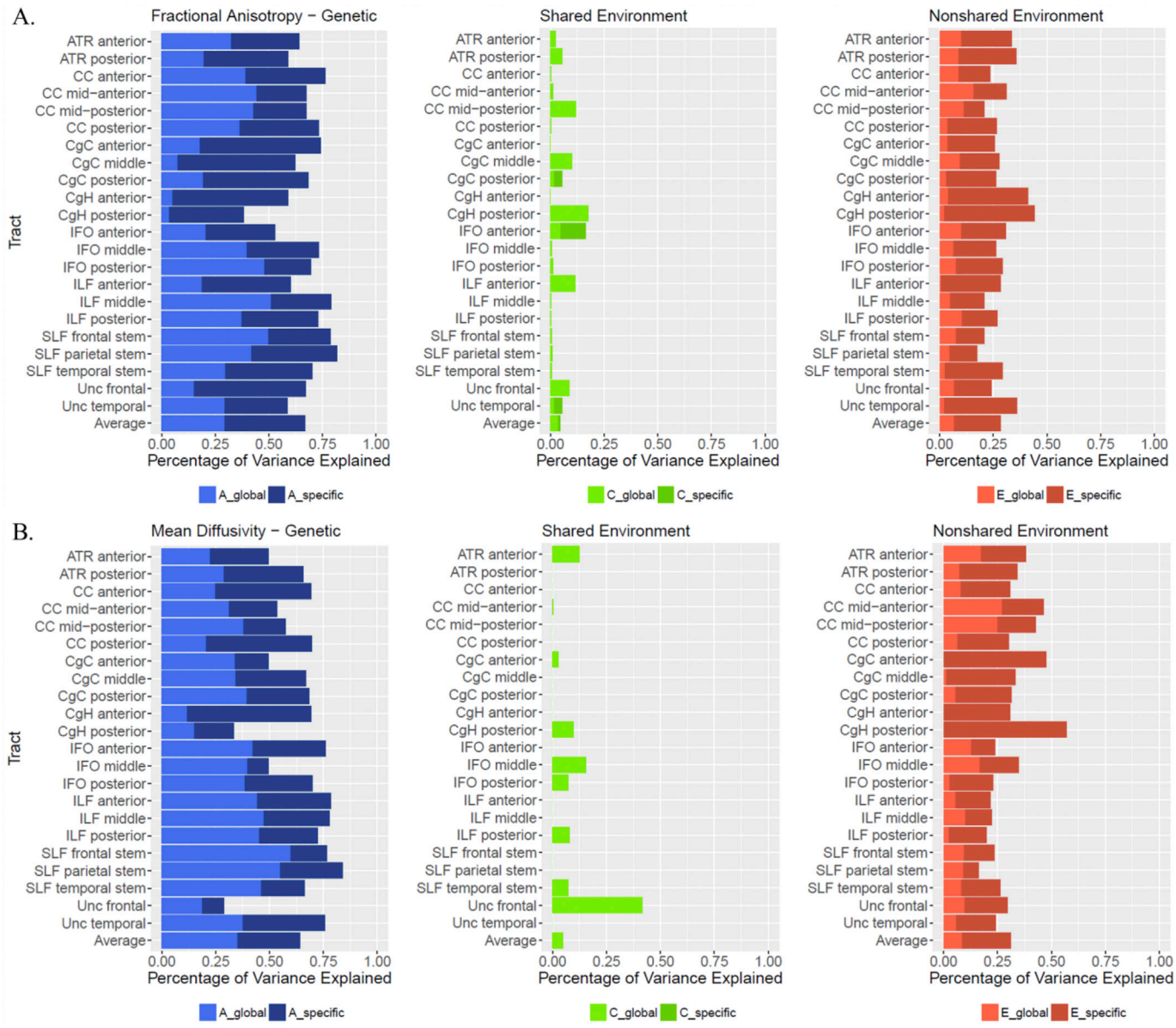

Fig. 4. Summary of the genetic (A), shared environmental (C), and non-shared environmental influences (E) on each of the 22 white matter tract subdivisions. As in Fig. 3, each influence is decomposed into components shared with the global measure (lighter color), or unique to the tract subdivisions (darker color). Results for fractional anisotropy (FA) are displayed on top and results mean diffusivity are displayed on the bottom. In each panel, the lowest row displays the mean for all tracts. The actual estimates, the genetic/environmental correlations, and the results for axial and radial diffusivity are displayed in the supplement (Figure S2 and Tables S9-S12). ATR = Anterior thalamic radiation, CC = corpus callosum, CgC = Cingulum, cingulate gyrus portion, CgH = Cingulum, hippocampal portion, IFO = Inferior frontal occipital fasciculus, ILF = Inferior longitudinal fasciculus, SLF = Superior longitudinal fasciculus, Unc = Uncinate.

tract likely represent the contribution of multiple but independent genetic effects such as differential plasticity or regional timing of brain maturation (e.g. posterior to anterior brain maturation during adolescence and young adulthood; Croteau-Chonka et al., 2016). Regardless, these results suggest that the genetic associations between a given white matter tract and cognitive processes, behaviors, or disease phenotypes, may reflect a combination of global and/or specific genetic influences. In other words, without comparing with (or statistically controlling for) the relevant global metric, it is unclear whether an association between cognition, for instance, and a given tract reflects a unique association, and/or is explained by an association with global white matter microstructure.

These findings are also relevant to work on cognitive aging, as there is already some evidence that general factors explain increasingly larger proportions of variance in white matter microstructure with increasing age in middle-aged adults (aged 40–69 years; Cox et al., 2016). Furthermore, although Chiang et al. (2011) revealed heritability of FA may decline between adolescence and young adulthood, these findings suggest there is still considerable heritability of white matter microstructure in late middle age across all diffusions metrics.

These results may also be useful in guiding ongoing efforts to use genome-wide association studies to identify specific genes underlying white matter microstructure. Analyses of global DTI measures are valuable for identifying genetic influences that underlie white matter variations across the entire brain. Because it is difficult to disentangle the common and specific sources of genetic variance with unadjusted tract-based measures, it would be beneficial to explore associations with specific tracts with and without adjusting for the global measure of the relevant DTI metric. Adjusting for global diffusion measures is analogous to examining regional cortical thickness after adjusting for mean

Table 3
Estimates and 95% Confidence Intervals for the Genetic and Environmental Components of Variance in FA and MD that are Shared with Global Measures and that are Specific to Each Tract.

Tracts	Fractional Anisotropy (FA)						Mean Diffusivity (MD)					
	a^2 global	a^2 specific	c^2 global	c^2 specific	e^2 global	e^2 specific	a^2 global	a^2 specific	c^2 global	c^2 specific	e^2 global	e^2 specific
ATR	0.33	0.32	0.02	0.00	0.13	0.20	0.43	0.27	0.01	0.00	0.13	0.16
	[.10, .50]	[.08, .48]	[.00, .30]	[.00, .28]	[.06, .23]	[.15, .28]	[.23, .59]	[.06, .36]	[.00, .28]	[.00, .22]	[.07, .23]	[.12, .22]
CC	0.64	0.17	0.00	0.00	0.14	0.05	0.53	0.20	0.00	0.00	0.21	0.06
	[.31, .74]	[.08, .22]	[.00, .33]	[.00, .10]	[.09, .22]	[.04, .07]	[.30, .63]	[.11, .25]	[.00, .24]	[.00, .09]	[.14, .32]	[.04, .09]
CgC	0.16	0.50	0.11	0.00	0.08	0.14	0.47	0.25	0.00	0.00	0.02	0.26
	[.01, .33]	[.28, .63]	[.00, .43]	[.00, .17]	[.04, .15]	[.10, .21]	[.30, .61]	[.09, .35]	[.00, .19]	[.00, .12]	[.00, .07]	[.19, .35]
CgH	0.06	0.50	0.02	0.00	0.05	0.37	0.17	0.42	0.00	0.00	0.01	0.39
	[.00, .20]	[.08, .62]	[.00, .42]	[.00, .35]	[.01, .14]	[.27, .50]	[.03, .29]	[.14, .55]	[.00, .33]	[.00, .21]	[.00, .07]	[.29, .53]
IFO	0.53	0.23	0.01	0.00	0.12	0.12	0.63	0.17	0.00	0.00	0.11	0.09
	[.27, .68]	[.09, .31]	[.00, .24]	[.00, .12]	[.07, .20]	[.08, .16]	[.46, .74]	[.07, .22]	[.00, .17]	[.00, .08]	[.06, .19]	[.07, .13]
IFSFC	0.54	0.27	0.00	0.00	0.11	0.07	0.61	0.23	0.00	0.00	0.11	0.06
	[.28, .64]	[.19, .33]	[.00, .27]	[.00, .07]	[.07, .18]	[.05, .10]	[.46, .70]	[.16, .28]	[.00, .14]	[.00, .05]	[.06, .17]	[.04, .08]
ILF	0.47	0.34	0.00	0.00	0.06	0.12	0.61	0.22	0.01	0.00	0.07	0.09
	[.25, .65]	[.16, .45]	[.00, .20]	[.00, .13]	[.03, .12]	[.09, .18]	[.44, .78]	[.06, .31]	[.00, .18]	[.00, .14]	[.03, .13]	[.06, .13]
SCS	0.21	0.40	0.24	0.00	0.04	0.11	0.60	0.17	0.00	0.00	0.13	0.08
	[.04, .45]	[.19, .61]	[.00, .52]	[.00, .33]	[.02, .08]	[.08, .16]	[.45, .73]	[.08, .24]	[.00, .13]	[.00, .06]	[.08, .22]	[.06, .12]
SIFC	0.46	0.18	0.10	0.00	0.10	0.15	0.55	0.23	0.00	0.00	0.13	0.10
	[.16, .65]	[.01, .37]	[.00, .44]	[.00, .29]	[.05, .17]	[.11, .21]	[.29, .65]	[.11, .29]	[.00, .30]	[.00, .11]	[.07, .21]	[.07, .13]
SLF	0.51	0.33	0.01	0.00	0.08	0.07	0.62	0.22	0.00	0.00	0.10	0.06
	[.30, .64]	[.22, .40]	[.00, .21]	[.00, .07]	[.05, .14]	[.05, .10]	[.47, .72]	[.14, .28]	[.00, .13]	[.00, .05]	[.06, .17]	[.04, .09]
Unc	0.21	0.35	0.20	0.00	0.06	0.18	0.30	0.22	0.27	0.00	0.09	0.12
	[.03, .45]	[.14, .49]	[.00, .52]	[.00, .17]	[.02, .12]	[.13, .25]	[.09, .54]	[.06, .39]	[.00, .56]	[.00, .19]	[.04, .16]	[.09, .17]

Note: ATR = Anterior thalamic radiation, CC = corpus callosum, CgC = Cingulum, cingulate gyrus portion, CgH = Cingulum, hippocampal portion, IFO = Inferior frontal occipital fasciculus, IFSFC = Inferior frontal superior frontal cortex, ILF = Inferior longitudinal fasciculus, SCS = superior corticostriate, SLF = Superior longitudinal fasciculus, SIFC = Striatal inferior frontal cortex, Unc = Uncinate.

Table 4
Estimates and 95% Confidence Intervals for the Genetic and Environmental Components of Variance in AD and RD that are Shared with Global Measures and that are Specific to Each Tract.

Tracts	Axial Diffusivity (AD)						Radial Diffusivity (RD)					
	a^2 global	a^2 specific	c^2 global	c^2 specific	e^2 global	e^2 specific	a^2 global	a^2 specific	c^2 global	c^2 specific	e^2 global	e^2 specific
ATR	0.46	0.31	0.00	0.00	0.05	0.18	0.41	0.23	0.03	0.00	0.16	0.17
	[.30, .61]	[.11, .40]	[.00, .22]	[.00, .17]	[.02, .12]	[.13, .25]	[.19, .58]	[.03, .38]	[.00, .30]	[.00, .25]	[.09, .27]	[.12, .23]
CC	0.47	0.24	0.00	0.00	0.21	0.08	0.56	0.19	0.00	0.00	0.20	0.06
	[.24, .57]	[.13, .30]	[.00, .27]	[.00, .27]	[.14, .33]	[.05, .11]	[.31, .67]	[.09, .24]	[.00, .26]	[.00, .10]	[.13, .30]	[.04, .08]
CgC	0.13	0.57	0.00	0.00	0.01	0.29	0.40	0.35	0.03	0.00	0.05	0.17
	[.05, .28]	[.29, .68]	[.00, .21]	[.00, .21]	[.00, .05]	[.21, .42]	[.14, .54]	[.16, .46]	[.00, .38]	[.00, .16]	[.02, .10]	[.12, .23]
CgH	0.17	0.34	0.00	0.00	0.00	0.49	0.07	0.31	0.24	0.00	0.03	0.35
	[.08, .31]	[.11, .50]	[.00, .14]	[.00, .13]	[.00, .04]	[.35, .66]	[.00, .25]	[.00, .58]	[.00, .61]	[.00, .38]	[.00, .10]	[.26, .48]
IFO	0.47	0.32	0.00	0.00	0.08	0.12	0.61	0.17	0.00	0.00	0.12	0.10
	[.33, .65]	[.12, .40]	[.00, .19]	[.00, .17]	[.04, .15]	[.09, .17]	[.41, .72]	[.07, .22]	[.00, .19]	[.00, .08]	[.07, .21]	[.08, .14]
IFSFC	0.53	0.24	0.06	0.00	0.08	0.09	0.58	0.25	0.00	0.00	0.11	0.06
	[.34, .70]	[.09, .39]	[.00, .27]	[.00, .21]	[.04, .14]	[.07, .13]	[.40, .66]	[.19, .31]	[.00, .16]	[.00, .04]	[.07, .18]	[.04, .09]
ILF	0.41	0.36	0.04	0.00	0.08	0.11	0.59	0.24	0.00	0.00	0.06	0.11
	[.22, .56]	[.18, .49]	[.00, .29]	[.00, .22]	[.04, .14]	[.08, .16]	[.43, .78]	[.06, .32]	[.00, .15]	[.00, .11]	[.03, .12]	[.07, .15]
SCS	0.42	0.32	0.02	0.00	0.10	0.13	0.48	0.35	0.00	0.00	0.09	0.08
	[.25, .61]	[.11, .45]	[.00, .22]	[.00, .21]	[.05, .19]	[.09, .19]	[.30, .63]	[.20, .43]	[.00, .20]	[.00, .13]	[.05, .15]	[.06, .12]
SIFC	0.46	0.24	0.09	0.00	0.09	0.12	0.51	0.24	0.01	0.00	0.13	0.11
	[.24, .63]	[.07, .38]	[.00, .36]	[.00, .23]	[.04, .16]	[.09, .17]	[.24, .64]	[.09, .32]	[.00, .34]	[.00, .15]	[.07, .21]	[.08, .16]
SLF	0.46	0.32	0.00	0.00	0.11	0.10	0.58	0.27	0.00	0.00	0.09	0.06
	[.30, .61]	[.15, .41]	[.00, .21]	[.00, .21]	[.06, .19]	[.07, .14]	[.42, .68]	[.18, .34]	[.00, .15]	[.00, .05]	[.05, .15]	[.04, .09]
Unc	0.30	0.32	0.03	0.00	0.09	0.26	0.21	0.23	0.38	0.00	0.08	0.11
	[.13, .48]	[.02, .45]	[.00, .33]	[.00, .28]	[.03, .19]	[.19, .36]	[.04, .47]	[.07, .41]	[.00, .63]	[.00, .18]	[.04, .15]	[.08, .15]

Note: ATR = Anterior thalamic radiation, CC = corpus callosum, CgC = Cingulum, cingulate gyrus portion, CgH = Cingulum, hippocampal portion, IFO = Inferior frontal occipital fasciculus, IFSFC = Inferior frontal superior frontal cortex, ILF = Inferior longitudinal fasciculus, SCS = superior corticostriate, SLF = Superior longitudinal fasciculus, SIFC = Striatal inferior frontal cortex, Unc = Uncinate.

thickness or examining regional cortical surface area after adjusting for total surface area (Vuoksimaa et al., 2017), although it remains unclear the most appropriate statistical approach to controlling for global measures.

In contrast to genetic influences, shared environmental influences were nonsignificant for either global or tract-specific influences regardless of the DTI metric. The lack of shared environmental influences is consistent with other measures of brain structure (Giedd et al., 2007; Peper et al., 2007; Pfefferbaum et al., 2000), and our earlier work (Vuoksimaa et al., 2017). Non-shared environmental influences explained a modest proportion of variance, and although comparatively smaller than for genetic influences, they also demonstrated some global and tract-specific components. This could reflect effects of global and specific measurement error, or the contribution of true environmental factors that generate variation in global and tract-specific white matter.

A potential limitation of the study is that the results displayed in Figs. 2 and 3 may be influenced by the relative size of tracts, given that large tracts might be more strongly associated with the global measure

simply because of their greater size. However, this does not entirely account for these results. First, the corpus callosum is the largest tract, yet it exhibited a comparable degree of tract-specific variance after global adjustment as other tracts (especially for MD). In an additional analysis, we also adjusted for a global measure of FA that excluded the corpus callosum. Even when the corpus callosum was excluded from the global measure, global FA still accounted for 32% of the variance in the corpus callosum (total heritability = 80%). Although variation in structure across the corpus callosum may have influenced these findings (Kanchibhotla et al., 2014), we suspect that similar results would be observed for other tracts if we had used a similar leave-one-out method in the analyses of each tract. Furthermore, the size of the region being averaged over might account for the findings that global influences accounted for a larger proportion of the genetic variance in tracts (e.g., 53% for FA) than subtracts (45% for FA). Voxel-wise analyses may have yielded different results, and the proportion of variance explained by global influences may vary more widely in smaller regions of interest (Eyler et al., 2012). Again, a key point here is that the regional specificity of relationships between white matter microstructure metrics and other measures may be misinterpreted if the relevant global diffusion measure is not taken into account.

Finally, it is important to acknowledge some limitations of the generalizability of the study. First, this sample comprised only men, who may demonstrate higher heritability than females, at least for FA (Chiang et al., 2011). Second, the sample was based on veterans, although most individuals did not report combat exposure and served in the military approximately 4 decades earlier. Rates of post-traumatic stress disorder symptoms and alcohol use problems were similar to those in the general population (Reynolds et al., 2015). Rates of traumatic brain injury (27%) were also similar to the median estimate for males (24%) across 14 studies of adults from the general population (Frost et al., 2013). Furthermore, the results were unchanged after repeating the primary analyses controlling for combat exposure. Nevertheless, it will be important to replicate these findings in other samples from the general population. Third, although we used conventional high resolution, low noise diffusion-weighted sequences, it will be useful for future investigations to replicate this analysis using next generation, multi-shell diffusion protocols (e.g. restricted spectrum imaging (RSI) or neurite orientation dispersion and density imaging (NODDI)) to overcome conventional DTI limitations in regions of cross fibers and to characterize different cellular compartments (e.g. intracellular vs extracellular diffusivity, etc).

5. Conclusion

The genetic and environmental influences on white matter microstructure demonstrate substantial diversity throughout the brain. However, global measures of FA, MD, AD, and RD appear to account for a substantial proportion of variation across all tracts. Accordingly, it is important to control for global diffusion measures when making inferences on associations with white matter microstructure in specific tracts, subdivisions, or brain regions.

Acknowledgements

This research was supported by Grants R01 AG050595, R01 AG018386, R01 AG018384, R01 AG022381, and K08 AG047903 from the National Institutes of Health.

The content of this manuscript is the responsibility of the authors and does not represent official views of NIA/NIH, or the Veterans' Administration. Numerous organizations provided invaluable assistance in the conduct of the VET Registry, including: U.S. Department of Veterans Affairs, Department of Defense; National Personnel Records Center, National Archives and Records Administration; Internal Revenue Service; National Opinion Research Center; National Research Council, National Academy of Sciences; the Institute for Survey Research, Temple University. The authors gratefully acknowledge the continued cooperation of the twins and the efforts of many staff members.

Appendix A. Supplementary data

Supplementary data to this article can be found online at https://doi.org/10.1016/j.neuroimage.2018.10.016.

References

Alexander, A.L., Hurley, S.A., Samsonov, A.A., Adluru, N., Hosseinbor, A.P., Mossahebi, P., et al., 2011. Characterization of cerebral white matter properties using quantitative magnetic resonance imaging stains. Brain Connect. 1, 423–446. https://doi.org/10.1089/brain.2011.0071.

Alexander, A.L., Lee, J.E., Lazar, M., Field, A.S., 2007. Diffusion tensor imaging of the brain. Neurotherapeutics 4, 316–329. https://doi.org/10.1016/j.nurt.2007.05.011.

Bennett, I.J., Madden, D.J., 2014. Disconnected aging: cerebral white matter integrity and age-related differences in cognition. Neuroscience 276, 187–205. https://doi.org/10.1016/j.neuroscience.2013.11.026.

Charlton, R.A., Barrick, T.R., McIntyre, D.J., Shen, Y., O'Sullivan, M., Howe, F.A., et al., 2006. White matter damage on diffusion tensor imaging correlates with age-related cognitive decline. Neurology 66, 217–222. https://doi.org/10.1212/01.wnl.0000194256.15247.83.

Chen, C.I., Mar, S., Brown, S., Song, S.K., Benzinger, T.L., 2011. Neuropathologic correlates for diffusion tensor imaging in postinfectious encephalopathy. Pediatr. Neurol. 44, 389–393. https://doi.org/10.1016/j.pediatrneurol.2010.12.007.

Chiang, M.C., McMahon, K.L., de Zubicaray, G.I., Martin, N.G., Hickie, I., Toga, A.W., et al., 2011. Genetics of white matter development: a DTI study of 705 twins and their siblings aged 12 to 29. Neuroimage 54, 2308–2317. https://doi.org/10.1016/j.neuroimage.2010.10.015.

Cox, S.R., Ritchie, S.J., Tucker-Drob, E.M., Liewald, D.C., Hagenaars, S.P., Davies, G., et al., 2016. Ageing and brain white matter structure in 3,513 UK Biobank participants. Nat. Commun. 7, 13629. https://doi.org/10.1038/ncomms13629.

Croteau-Chonka, E.C., Dean, D.C., Remer, J., Dirks, H., O'Muircheartaigh, J., Deoni, S.C.L., 2016. Examining the relationships between cortical maturation and white matter myelination throughout early childhood. Neuroimage 125, 413–421. https://doi.org/10.1016/j.neuroimage.2015.10.038.

Eyler, L.T., Chen, C.H., Panizzon, M.S., Fennema-Notestine, C., Neale, M.C., Jak, A., et al., 2012. A comparison of heritability maps of cortical surface area and thickness and the influence of adjustment for whole brain measures: a magnetic resonance imaging twin study. Twin Res. Hum. Genet. 15, 304–314. https://doi.org/10.1017/thg.2012.3.

Freund, P., Wheeler-Kingshott, C.A., Nagy, Z., Gorgoraptis, N., Weiskopf, N., Friston, K., et al., 2012. Axonal integrity predicts cortical reorganisation following cervical injury. J. Neurol. Neurosurg. Psychiatry 83, 629–637. https://doi.org/10.1136/jnnp-2011-301875.

Frost, R.B., Farrer, T.J., Primosch, M., Hedges, D.W., 2013. Prevalence of traumatic brain injury in the general adult population: a meta-analysis. Neuroepidemiology 40, 154–159. https://doi.org/10.1159/000343275.

Giedd, J.N., Schmitt, J.E., Neale, M.C., 2007. Structural brain magnetic resonance imaging of pediatric twins. Hum. Brain Mapp. 28, 474–481. https://doi.org/10.1002/hbm.20403.

Hagler Jr., D.J., Ahmadi, M.E., Kuperman, J., Holland, D., McDonald, C.R., Halgren, E., Dale, A.M., 2009. Automated white-matter tractography using a probabilistic diffusion tensor atlas: application to temporal lobe epilepsy. Hum. Brain Mapp. 30, 1535–1547. https://doi.org/10.1002/hbm.20619.

Harsan, L.A., Poulet, P., Guignard, B., Steibel, J., Parizel, N., de Sousa, P.L., et al., 2006. Brain dysmyelination and recovery assessment by noninvasive in vivo diffusion tensor magnetic resonance imaging. J. Neurosci. Res. 83, 392–402. https://doi.org/10.1002/jnr.20742.

Hatton, S.N., Panizzon, M.S., Vuoksimaa, E., Hagler, D.J., Fennema-Notestine, C., Rinker, D., et al., 2018. Genetic relatedness of axial and radial diffusivity indices of cerebral white matter microstructure in late middle age. Hum. Brain Mapp. https://doi.org/10.1002/hbm.24002 advance online publication.

Holland, D., Kuperman, J.M., Dale, A.M., 2010. Efficient correction of inhomogeneous static magnetic field-induced distortion in Echo Planar Imaging. Neuroimage 50, 175–183. https://doi.org/10.1016/j.neuroimage.2009.11.044.

Hollingshead, A.B., 1975. Four Factor Index of Social Status. Yale University, New Haven, CT.

Jahanshad, N., Kochunov, P.V., Sprooten, E., Mandl, R.C., Nichols, T.E., Almasy, L., et al., 2013. Multi-site genetic analysis of diffusion images and voxelwise heritability analysis: a pilot project of the ENIGMA-DTI working group. Neuroimage 81, 455–469. https://doi.org/10.1016/j.neuroimage.2013.04.061.

Janes, G.R., Goldberg, J., Eisen, S.A., True, W.R., 1991. Reliability and validity of a combat exposure index for vietnam era verterans. J. Clin. Psychol. 47, 80–86. https://doi.org/10.1002/1097-4679(199101)47:1<80::aid-jclp2270470112>3.0.co;2-9.

Jovicich, J., Czanner, S., Greve, D., Haley, E., van der Kouwe, A., Gollub, R., et al., 2006. Reliability in multi-site structural MRI studies: effects of gradient non-linearity correction on phantom and human data. Neuroimage 30, 436–443. https://doi.org/10.1016/j.neuroimage.2005.09.046.

Kanchibhotla, S.C., Mather, K.A., Thalamuthu, A., Zhuang, L., Schofield, P.R., Kwok, J.B., et al., 2014. Genetics of microstructure of the corpus callosum in older adults. PloS One 9, e113181. https://doi.org/10.1371/journal.pone.0113181.

Kaup, A., Toomey, R., Bangen, K.J., Delano-Wood, L., Yaffe, K.C., Panizzon, M.S., et al., 2018. The interactive effect of traumatic brain injury and psychiatric symptoms on cognition among late middle-aged men: findings from the Vietnam Era twin study of aging (VETSA). J. Neurotrauma. https://doi.org/10.1089/neu.2018.5695.

Klawiter, E.C., Xu, J., Naismith, R.T., Benzinger, T.L., Shimony, J.S., Lancia, S., et al., 2012. Increased radial diffusivity in spinal cord lesions in neuromyelitis optica compared with multiple sclerosis. Mult. Scler. 18, 1259–1268. https://doi.org/10.1177/1352458512436593.

Kochunov, P., Fu, M., Nugent, K., Wright, S.N., Du, X., Muellerklein, F., et al., 2016. Heritability of complex white matter diffusion traits assessed in a population isolate. Hum. Brain Mapp. 37, 525–535. https://doi.org/10.1002/hbm.23047.

Koenen, K.C., Lyons, M.J., Goldberg, J., Simpson, J., Williams, W.M., Toomey, R., et al., 2003. Co-twin control study of relationships among combat exposure, combat-related PTSD, and other mental disorders. J. Trauma Stress 16, 433–438. https://doi.org/10.1023/A:1025786925483.

Kremen, W.S., Panizzon, M.S., Xian, H., Barch, D.M., Franz, C.E., Grant, M.D., et al., 2011. Genetic architecture of context processing in late middle age: more than one underlying mechanism. Psychol. Aging 26, 852–863. https://doi.org/10.1037/a0025098.

Kremen, W.S., Thompson-Brenner, H., Leung, Y.M., Grant, M.D., Franz, C.E., Eisen, S.A., et al., 2006. Genes, environment, and time: the Vietnam Era twin study of aging (VETSA). Twin Res. Hum. Genet. 9, 1009–1022. https://doi.org/10.1375/183242706779462750.

Lee, S.J., Steiner, R.J., Yu, Y., Short, S.J., Neale, M.C., Styner, M.A., et al., 2017. Common and heritable components of white matter microstructure predict cognitive function at 1 and 2 y. Proc. Natl. Acad. Sci. U. S. A. 114, 148–153. https://doi.org/10.1073/pnas.1604658114.

Mabbott, D.J., Noseworthy, M.D., Bouffet, E., Rockel, C., Laughlin, S., 2006. Diffusion tensor imaging of white matter after cranial radiation in children for medulloblastoma: correlation with IQ. Neuro Oncol. 8, 244–252. https://doi.org/10.1215/15228517-2006-002.

Mayfield, D., McLeod, G., Hall, P., 1974. The CAGE questionnaire: validation of a new alcoholism screening instrument. Am. J. Psychiatry 131, 1121–1123. https://doi.org/10.1176/ajp.131.10.1121.

McEvoy, L.K., Fennema-Notestine, C., Eyler, L.T., Franz, C.E., Hagler Jr., D.J., Lyons, M.J., et al., 2015. Hypertension-related alterations in white matter microstructure detectable in middle age. Hypertension 66, 317–323. https://doi.org/10.1161/HYPERTENSIONAHA.115.05336.

Naismith, R.T., Xu, J., Tutlam, N.T., Scully, P.T., Trinkaus, K., Snyder, A.Z., et al., 2010. Increased diffusivity in acute multiple sclerosis lesions predicts risk of black hole. Neurology 74, 1694–1701. https://doi.org/10.1212/WNL.0b013e3181e042c4.

Neale, M.C., Cardon, L.R., 1992. Methodology for Genetic Studies of Twins and Families. Kluwer Academic Publishers, Dordrecht.

Neale, M.C., Hunter, M.D., Pritikin, J.N., Zahery, M., Brick, T.R., Kirkpatrick, R.M., et al., 2016. OpenMx 2.0: extended structural equation and statistical modeling. Psychometrika 81, 535–549. https://doi.org/10.1007/s11336-014-9435-8.

Peper, J.S., Brouwer, R.M., Boomsma, D.I., Kahn, R.S., Hulshoff Pol, H.E., 2007. Genetic influences on human brain structure: a review of brain imaging studies in twins. Hum. Brain Mapp. 28, 464–473. https://doi.org/10.1002/hbm.20398.

Pfefferbaum, A., Sullivan, E.V., Swan, G.E., Carmelli, D., 2000. Brain structure in men remains highly heritable in the seventh and eighth decades of life. Neurobiol. Aging 21, 63–74.

Reynolds, K., Pietrzak, R.H., El-Gabalawy, R., Mackenzie, C.S., Sareen, J., 2015. Prevalence of psychiatric disorders in U.S. older adults: findings from a nationally representative survey. World Psychiatr. 14, 74–81. https://doi.org/10.1002/wps.20193.

Schoenborn, C.A., Heyman, K.M., 2009. Health characteristics of adults aged 55 years and over: United States, 2004-2007. In: National Health Statistics Report, 16, pp. 1–31.

Sled, J.G., Zijdenbos, A.P., Evans, A.C., 1998. A nonparametric method for automatic correction of intensity nonuniformity in MRI data. IEEE Trans. Med. Imag. 17, 87–97. https://doi.org/10.1109/42.668698.

Song, S.K., Sun, S.W., Ramsbottom, M.J., Chang, C., Russell, J., Cross, A.H., 2002. Dysmyelination revealed through MRI as increased radial (but unchanged axial) diffusion of water. Neuroimage 17, 1429–1436. https://doi.org/10.1006/nimg.2002.1267.

Song, S.K., Yoshino, J., Le, T.Q., Lin, S.J., Sun, S.W., Cross, A.H., Armstrong, R.C., 2005. Demyelination increases radial diffusivity in corpus callosum of mouse brain. Neuroimage 26, 132–140. https://doi.org/10.1016/j.neuroimage.2005.01.028.

Sun, S.W., Liang, H.F., Trinkaus, K., Cross, A.H., Armstrong, R.C., Song, S.K., 2006. Noninvasive detection of cuprizone induced axonal damage and demyelination in the mouse corpus callosum. Magn. Reson. Med. 55, 302–308. https://doi.org/10.1002/mrm.20774.

Tsuang, M.T., Bar, J.L., Harley, R.M., Lyons, M.J., 2001. The harvard twin study of substance abuse: what we have learned. Harv. Rev. Psychiatr. 9, 267–279. https://doi.org/10.1093/hrp/9.6.267.

Tyszka, J.M., Readhead, C., Bearer, E.L., Pautler, R.G., Jacobs, R.E., 2006. Statistical diffusion tensor histology reveals regional dysmyelination effects in the shiverer mouse mutant. Neuroimage 29, 1058–1065. https://doi.org/10.1016/j.neuroimage.2005.08.037.

Vuoksimaa, E., Panizzon, M.S., Hagler Jr., D.J., Hatton, S.N., Fennema-Notestine, C., Rinker, D., et al., 2017. Heritability of white matter microstructure in late middle age: a twin study of tract-based fractional anisotropy and absolute diffusivity indices. Hum. Brain Mapp. 38, 2026–2036. https://doi.org/10.1002/hbm.23502.

Weathers, F.W., Litz, B.T., Herman, D.S., Huska, J.A., Keane, T.M., 1993. The PTSD Checklist (PCL): reliability, validity, and diagnostic utility. In: Paper Presented at the the 9th Annual Meeting of the International Society for Traumatic Stress Studies.

Wells 3rd, W.M., Viola, P., Atsumi, H., Nakajima, S., Kikinis, R., 1996. Multi-modal volume registration by maximization of mutual information. Med. Image Anal. 1, 35–51.

Westlye, L.T., Walhovd, K.B., Dale, A.M., Bjornerud, A., Due-Tonnessen, P., Engvig, A., et al., 2010. Life-span changes of the human brain white matter: diffusion tensor imaging (DTI) and volumetry. Cerebr. Cortex 20, 2055–2068. https://doi.org/10.1093/cercor/bhp280.

Zhang, J., Jones, M., DeBoy, C.A., Reich, D.S., Farrell, J.A., Hoffman, P.N., et al., 2009. Diffusion tensor magnetic resonance imaging of Wallerian degeneration in rat spinal cord after dorsal root axotomy. J. Neurosci. 29, 3160–3171. https://doi.org/10.1523/JNEUROSCI.3941-08.2009.

Zhuang, J., Hrabe, J., Kangarlu, A., Xu, D., Bansal, R., Branch, C.A., Peterson, B.S., 2006. Correction of eddy-current distortions in diffusion tensor images using the known directions and strengths of diffusion gradients. J. Magn. Reson. Imag. 24, 1188–1193. https://doi.org/10.1002/jmri.20727.